








Superconductivity in dense scandium-based phosphides

Kaixuan Zhao ¹, Qianyi Wang ¹, Honggang Li ¹, Bo Gao ², Shubo Wei,³ Li Zhu ⁴, Haiyang Xu,¹
Hanyu Liu ^{3,*} and Shoutao Zhang ^{1,†}

¹Key Laboratory of UV-Emitting Materials and Technology of Ministry of Education, School of Physics, Northeast Normal University, Changchun 130024, China

²College of Materials Science and Engineering, Jilin University, Changchun 130022, China

³Key Laboratory of Material Simulation Methods and Software of Ministry of Education & State Key Laboratory of Superhard Materials, College of Physics, Jilin University, Changchun 130012, China

⁴Department of Physics, Rutgers University, Newark, New Jersey 07102, USA



(Received 25 April 2023; revised 7 August 2023; accepted 1 November 2023; published 22 November 2023)

The recent achievement of room-temperature superconductivity at near-ambient pressure in nitrogen-doped lutetium hydride further boosts enthusiasm for the pursuit of high-temperature superconductors. Transition-metal phosphides (TMPs) have attracted substantial attention due to their fascinating properties encompassing superconductivity. Nevertheless, the superconducting scandium-based phosphides with high scandium concentration are not well comprehended. Towards this end, our work focuses on the rational design of scandium-rich phosphides via the first-principles swarm structure calculations under pressure. Strikingly, several metallic phases, viz., ScP, Sc₂P, and Sc₃P, are unambiguously uncovered wherein P atoms exhibit captivating configurations from ladder, linear chain, and eventually to isolated atom. Further electron-phonon coupling simulations elucidate that *P6/mmm* Sc₂P, isostructural to MgB₂, possesses a remarkable superconducting transition temperature, T_c , of ~ 20 K at 100 GPa, mainly deriving from the large acoustic phonon softening in the low-frequency region. Tetragonal *I4/mmm* Sc₃P is revealed to host a high phonon-mediated superconductivity of 20.5 K at 140 GPa, which is chiefly attributed to the significant coupling between the low-frequency softened acoustic and optical phonon modes associated with the Sc-dominated vibrations and Sc *3d* electronic states around the Fermi energy. This study paves the way for discovering distinguished superconductors in transition metal-based phosphide systems.

DOI: [10.1103/PhysRevB.108.174513](https://doi.org/10.1103/PhysRevB.108.174513)

I. INTRODUCTION

The design of novel superconductors with intriguing structure features and high-temperature superconductivity has been a research hotspot in the fields of condensed-matter physics, chemistry, and materials science [1–5]. Recently, plenty of pressure-stabilized high- T_c hydrogen-rich compounds with peculiar hydrogen structures have been predicted [6–10]. Several hydrides are successfully synthesized such as covalent hydride H₃S with 203 K at 155 GPa [11], clathrate superhydrides CaH₆ (215 K at 172 GPa [12], 210 K at 160 GPa [13]), LaH₁₀ (250 K at 170 GPa [14], 260 K at 188 GPa [15]) and currently reported room-temperature superconductor N-doped lutetium hydride at near-ambient pressure (294 K at 10 kbar) [16], demonstrating the critical role of the theoretical calculations in revealing emerging superconductive materials.

Furthermore, transition-metal phosphides are of great importance in industrial applications such as energy storage [17,18] and catalysts [19,20] and have emerged as a platform for possessing superconductivity [21–25] and striking phosphorus motifs [26–28] due to the rich valence electron configurations of transition-metal elements. For instance,

pressure-induced MnP with superconductivity of 1 K was discovered to be the first Mn-based superconductor [29]. Notable superconductivity at 5.5–7.0 K has been observed in Mo₃P [30–32]. Nb₂P₅ with zigzag-type infinite phosphorus chain is synthesized and occurs superconductive transition at 2.6 K [33]. Recently, pressure-stabilized *Fd-3m* YP₂ with unforeseen vertex-sharing P₄ tetrahedra exhibits superconductivity of 9.5 K, and *Pm-3m* Y₃P has a much higher estimated T_c of 12.1 K [34]. To date, MgB₂-structured LaP₂ with graphene-like P layer is reported to show the predicted highest T_c (22.2 K at 11 GPa) recorded in the transition-metal phosphides (TMPs) [35].

Scandium (Sc) is a member of transition metals, whose elemental materials are superconductors [36,37], and shows breakthrough superconductivity under extreme compression. Recently, record high- T_c superconductivity of elemental superconductors is achieved in compressed scandium (36 K at 260 GPa [38], 32 K at 283 GPa [39]). Meanwhile, binary compounds of Sc exhibit interesting properties comprising electronegativity [40] and superconductivity [41]. For example, the first 2D electronegative semiconductor Sc₂C was recently synthesized [42]. Also, striking superconductivity emerges in scandium compounds [43–46], such as, room-temperature superconductivity of 313 K, was predicted in a superhydride ScH₁₂ with quasiautomatic H₂ units below one megabar [47].

*Corresponding author: hanyuliu@jlu.edu.cn

†Corresponding author: zhangst966@nenu.edu.cn

With regards to the Sc-P compounds reported up to date, there are three metallic phases of *Fm-3m* ScP [48], *Pnma* Sc₃P₂ [49], and *Pnma* Sc₃P [50] at atmospheric conditions. More recently, several superconducting phases of *Pnma*-, *Cmmm*-, and *P4/mmm*-structured ScP, *Fddd* ScP₂, and *C2/m* ScP₄ are predicted under pressure below 300 GPa, where ScP₄ has a calculated T_c of 11 K at 50 GPa [51]. Subsequently, *Pmc2₁* ScP₃, *C2/m* ScP₂, *R-3m* ScP, *P6₃/mcm* Sc₅P₃, *Cmce* Sc₂P, *P6₃/m* Sc₂P, and *Pm-3m* Sc₃P are found by the structure search between 1 atm and 100 GPa, where Sc₅P₃ and Sc₃P are one-dimensional and zero-dimensional electrides [52], respectively. Meanwhile, Sc₅P₃ and Sc₃P have low work-function values of 2.64 and 2.57 eV, respectively. Although a series of compressed Sc-rich and P-rich Sc-P compounds with appealing properties have been identified, the phase diagram, structures, and superconductivity of scandium-rich phosphides in the broader pressure region remain yet unknown. It is well known that pressure, as a powerful research tool, plays a predominant role in identifying emerging materials [53–57]. Therefore, it is expected that scandium-rich phosphides in the Sc-P system can exhibit more diverse structures and remarkable superconductivity at elevated pressure.

In this work, we conduct comprehensive structure searches on Sc-P compounds with multiple Sc-rich Sc_{*m*}P_{*n*} compositions below 300 GPa and systematically establish the high-pressure phase diagram of scandium-rich phosphides. Several stable metallic phases (i.e., *Pbam* ScP, *P6/mmm* Sc₂P, *I4/mmm* Sc₃P, and *Im-3* Sc₃P) are determined wherein interesting ladderlike and linear-chain P arrangements are found in *Pbam* ScP and *P6/mmm* Sc₂P, respectively. Strikingly, *P6/mmm* Sc₂P not only hosts the MgB₂-type structure but also has significant superconducting critical temperature of 19.8 K at 1 Mbar. *I4/mmm* Sc₃P has a calculated T_c value of 20.5 K at 140 GPa, remarkable among binary transition metal-rich phosphides. Our work not only expands the family of transition-metal phosphides but also deepens the insights of the structures and superconducting properties of TMPs.

II. COMPUTATIONAL DETAILS

To attain stable Sc-rich Sc-P compounds with desirable properties, we performed structure searches of the Sc-P system under compression by using the highly efficient CALYPSO package [58,59], which has been successfully applied for discovering stable or metastable materials [53,60–69]. The calculations on structure relaxation and electronic structures were implemented via the Vienna *Ab initio* Simulation Package (VASP) code [70] based on density-functional theory [71,72]. The projector augmented-wave (PAW) [73] pseudopotentials with valence electron configurations of $3s^2 3p^6 3d^1 4s^2$ (Sc) and $3s^2 3p^3$ (P) were selected. The Perdew-Burke-Ernzerhof [74] functional of the generalized gradient approximation (GGA) [75] was adopted to describe the exchange-correlation interactions. A cutoff energy of 800 eV and choosing *k*-point grid [76] with a reciprocal-space resolution of $2\pi \times 0.03 \text{ \AA}^{-1}$ could ensure the convergence of total energies. Phonon spectra calculations were achieved by PHONOPY code [77] with the finite displacement method in the supercell [78]. Superconductive properties calculations

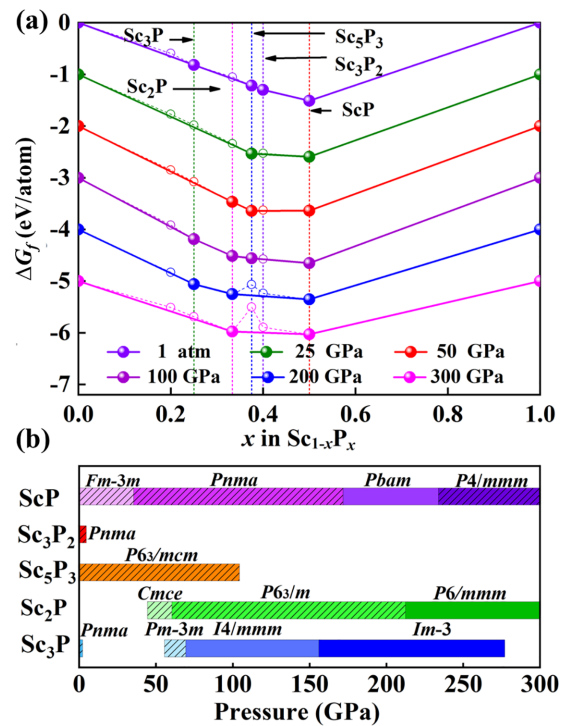


FIG. 1. Energetic stability of Sc-P system at selected pressures. (a) Convex hulls of diverse Sc-rich Sc_{*m*}P_{*n*} compounds with respect to elemental Sc and P solids. For clarity, formation energies of each composition at 25, 50, 100, 200, and 300 GPa are offset by -1.0 , -2.0 , -3.0 , -4.0 , and -5.0 eV, respectively. Here, *P6₃/mcm*, *Cmca*, *P6₁22*, and *P-1* structures of Sc [83–85] are exploited to calculate formation energies. *Cmca*, *Pm-3m*, *P6/mmm*, and *I-43d* phases of P [86–88] are taken into consideration. (b) Pressure-composition phase diagram of stable Sc-rich Sc-P phases. Stability pressure ranges of various Sc-P phases are denoted by different colored horizontal bars, where previously raised phases are represented by italicized lines.

adopting ultrasoft pseudopotentials were implemented via the QUANTUM ESPRESSO package [79]. More computation details are illustrated in Supplemental Material [80] (see also Refs. [81,82] therein).

III. RESULTS AND DISCUSSION

A. Stability of Sc-rich Sc-P phases

To study the phase stabilities of scandium-rich compounds in the Sc-P system, we carry out an extensive structural search on varying Sc_{*m*}P_{*n*} ($m = 1-4$, $n = 1$; $m = 3$, $n = 2$) compositions at the temperature of 0 K and consider pressures of 1 atm, 25, 50, 100, 200, and 300 GPa. Then, the relative energy stability of the lowest-energy structure of each composition with respect to the elemental phases of the constituent elements of Sc and P is calculated at corresponding pressure by using the following formula of formation energy $\Delta G_f(\text{Sc}_m\text{P}_n) = [G(\text{Sc}_m\text{P}_n) - mG(\text{Sc}) - nG(\text{P})]/(m + n)$ wherein $G(\text{Sc}_m\text{P}_n)$, $G(\text{Sc})$, and $G(\text{P})$ are the Gibbs free energies of Sc_{*m*}P_{*n*}, Sc, and P at the same pressure, respectively. Subsequently, the convex hull diagram is built by exploiting the above formation energies of the Sc_{*m*}P_{*n*} compounds [Fig. 1(a)]. The compounds

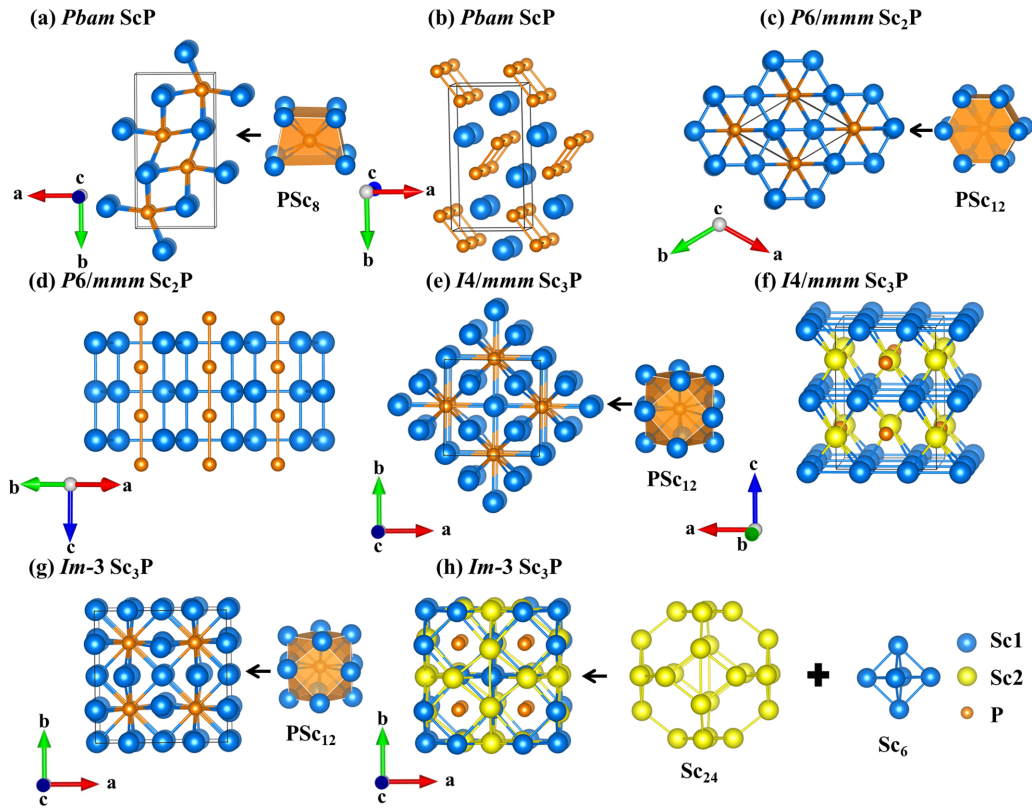


FIG. 2. Crystal structures of predicted stable Sc-P compounds. (a) *Pbam* ScP with PSc_8 polyhedron at 200 GPa. (b) Ladderlike P arrangement in *Pbam* ScP. (c) Polyhedron view of $P6/mmm$ Sc_2P in MgB_2 structure at 300 GPa. (d) One-dimensional P chain in $P6/mmm$ Sc_2P . (e) $I4/mmm$ Sc_3P containing PSc_{12} unit at 100 GPa. (f) $I4/mmm$ Sc_3P with scandium layer and isolated scandium atom. (g) $Im-3$ Sc_3P at 200 GPa with PSc_{12} -polyhedral unit. (h) Cage-type Sc_{24} structure and octahedral Sc_6 unit in $Im-3$ Sc_3P .

represented by the solid circles on the solid line are thermodynamically stable, whereas the ones signified by hollow circles located on dotted lines are metastable and easily decompose into other energetically stable chemical components. As shown in Fig. 1(a), four Sc-rich stoichiometric compounds encompassing ScP, Sc_3P_2 , Sc_5P_3 , Sc_2P , and Sc_3P are found to be energetically stable. Meanwhile, existing $Fm-3m$ ScP [48], $Pnma$ Sc_3P_2 [49], $P6_3/mcm$ Sc_5P_3 [52], and $Pnma$ Sc_3P [50] at 1 atm are rediscovered, demonstrating that the structure search simulations and adopted pseudopotentials are reliable. Moreover, the $P4/mbm$ Sc_3P_2 at 100 GPa, $P4/nmm$ Sc_2P at 25 GPa, $C2/m$ Sc_4P at 25 GPa, and $C2/c$ Sc_4P at 50 GPa selected (Fig. S1) are found to have relatively low positive formation energies of 6, 22, 47, and 29 meV per atom, respectively, relative to neighboring reference phases (Table S2), indicating that they are thermodynamically unstable. Meanwhile, they also satisfy dynamical stabilities as judged by no imaginary phonon frequencies (Fig. S2) and further exhibit metastability. Therefore, these four metastable phases are kinetically stable and accessible for experiments.

Furthermore, the pressure-composition phase diagram is well constructed by precisely determining the stable pressure regions of the scandium-rich phosphides [Fig. 1(b)]. As for ScP, based on the previously reported two phase transformation sequences ($Fm-3m \rightarrow Pnma \rightarrow Cmmm \rightarrow P4/nmm$) [51] and ($Fm-3m \rightarrow Pnma \rightarrow R-3m$) [52], we find an unreported *Pbam* ScP in the pressure range between 171.8 and 233.8 GPa (Fig. S3) and further confirm

the final phase-transition sequence ($Fm-3m \rightarrow Pnma \rightarrow Pbam \rightarrow P4/nmm$) below 300 GPa. As Sc concentration increases, in addition to the two known low-pressure phases $Cmce$ and $P6_3/m$ [52], a high-pressure phase with space group $P6/mmm$ of Sc_2P emerges above 212.1 GPa and maintains stability up to 300 GPa. For the most Sc-rich stable stoichiometry, the previously proposed $Pm-3m$ Sc_3P [52] transforms into the high-pressure phase $I4/mmm$ Sc_3P above 69.4 GPa and then converts to Sc_3P with higher symmetry of $Im-3$ at 156.1 GPa and further stabilizes up to 277.1 GPa. Also, the lattice dynamic stabilities of predicted stable *Pbam* ScP, $P6/mmm$ Sc_2P , $I4/mmm$ Sc_3P , and $Im-3$ Sc_3P phases are verified by calculating their phonon dispersion curves. It is noteworthy that they do conform to dynamic stabilities because of the absence of imaginary phonon frequencies in the Brillouin zone of the predicted structures (Fig. S4).

B. Geometrical motifs and chemical bonding

Interesting structural features are displayed in pressure-induced stable Sc-P phases. Here, we mainly focus on the structural analysis of our predicted Sc-P structures. For ScP stoichiometry, complicated phase transitions are found. It is worth noting that an energetically favorable orthorhombic ScP phase is proposed to have *Pbam* symmetry [Fig. 2(a)]. This structure has 4 formula units (f.u.) and can be viewed as a stack of PSc_8 hexahedron basic units with Sc-P distances of 2.30–2.37 Å at 200 GPa. Interestingly, P atoms form

quadrilaterals with P–P bond lengths of 2.05 and 2.26 Å at 200 GPa, and these quadrilaterals share edges along the *c* axis and constitute a ladderlike phosphorus sublattice [Fig. 2(b)].

For Sc₂P with higher Sc content, pressure induces an unprecedentedly stable hexagonal phase. Compared with the previously presented two low-pressure structures with space group of *Cmce* and *P6₃/m*, the hexagonal structure of Sc₂P has a higher symmetry of *P6/mmm*, wherein geometric configuration is similar to *P6/mmm*-structured MgB₂ [89], NaC₂ [66], and Li₂Si [90], (1 f.u. per cell, Fig. 2c). Meanwhile, this structure consists of PSc₁₂ octahedron with P–Sc distance of 2.32 Å at 300 GPa, where each P atoms have a higher coordination number of 12 than 8 of *Pbam*-structured ScP. Furthermore, Sc atoms form a honeycomb-like graphene structure in the *ab* plane, whereas the P atoms in *P6/mmm* Sc₂P make up the one-dimensional straight chains with P–P bond length of 2.19 Å at 300 GPa along the *c* axis [Fig. 2(d)]. Meanwhile, the special MgB₂-type structure is revealed in *P6/mmm* Sc₂P, indicating it has underlying superconductivity, which will be discussed later.

As for the stable Sc₃P composition with the highest Sc content, the high-pressure tetragonal structure of Sc₃P is found to have space group *I4/mmm* [4 f.u. per cell, Fig. 2(e)] and can be viewed as stacking of P-centered PSc₁₂ unit comprising 14 faces, where the distance between P and Sc is 2.53 Å at 100 GPa. Notably, *I4/mmm* Sc₃P has two kinds of occupations, i.e., Sc1 8*h* (0.7386, 0.7386, 0.0000) and Sc2 4*e* (0.0000, 0.0000, 0.7719). Sc1 atoms form planar sheet with Sc1–Sc1 distances of 2.40 and 2.63 Å, whereas isolated Sc2 atom is coordinated by 8 Sc1 atoms with distances of 2.48 and 2.58 Å [Fig. 2(f)]. Under further compression, Sc₃P adopts a cubic phase with a higher symmetry of *Im-3* [8 f.u. per cell, Fig. 2(g)]. In this structure, each P is embraced by 12 Sc atoms with bond lengths of 2.36 and 2.37 Å at 200 GPa and further constitutes the PSc₁₂ polyhedron including eight triangles and six square quadrilaterals. Two inequivalent Wyckoff positions of Sc atoms in *Im-3* Sc₃P are found in Fig. 2(h), namely, Sc1 12*d* (0.2507, 0.0000, 0.0000) and Sc2 12*e* (0.2203, 0.5000, 0.0000). Intriguingly, Sc1 atoms constitute the 24-membered Sc clathrate structure, which is analogous to H₂₄ cage of *Im-3m*-structured CaH₆ [65] and carbon-boron framework in synthesized cubic SrB₃C₃ [91]. By comparison, Sc2 atoms form Sc₆ octahedra, which is similar to B₆ octahedra in *I4/mmm* Na₂B₃ [92]. Furthermore, these two types of Sc structural units are interconnected to construct a three-dimensional network configuration.

To unveil the bonding features, the electron localization functions (ELF) [93] of *Pbam* ScP, *P6/mmm* Sc₂P, *I4/mmm* Sc₃P, and *Im-3* Sc₃P structures determined in this work are computed. As illustrated in Fig. S5, the bonding between Sc and P is ionic as evidenced by the apparent difference of the ELF values around Sc and P, which indicates the charge transfer from Sc to P atoms due to their electronegativity difference [94,95] and is further supported by the Bader charge analysis [96] (Table S3). Meanwhile, the evident electron localization between P atoms in *Pbam* ScP and *P6/mmm* Sc₂P is found and has the ELF value larger than 0.5, demonstrating that the strong covalent bond. On the basis, the structural stabilities of predicted Sc-rich Sc-P compounds are mainly ascribed to the strong ionic Sc–P and covalent P–P bonds.

C. Superconductive properties of MgB₂-type Sc₂P

The striking structures of predicted stable Sc-rich Sc-P phases further stimulate us to study their electronic structures. The metallic character of *Pbam* ScP at 200 GPa, *P6/mmm* Sc₂P at 300 GPa, *I4/mmm* Sc₃P at 100 GPa, and *Im-3* Sc₃P at 200 GPa is well revealed by the calculated electronic band structures and projected density of states (PDOS) (Fig. S6). Their notable metallicity inspires us to explore their superconductivity. Considering the unique structure of *P6/mmm* Sc₂P possessing MgB₂ configuration and potential superconductivity, we first focus on its superconducting investigation. As clearly depicted in the band structure of Sc₂P at 250 GPa in Figs. 3(a) and S7, four energy bands crossing the Fermi level E_f are found to show the obvious dispersion, leading to the emergence of the electron pockets below E_f . Furthermore, as shown in Figs. 3(a) and S7, band 1 and band 2 are found to have evident dispersion below the Fermi level along the Γ -*A* direction compared to other directions in the Brillouin zone. Band 3 and band 4 exhibit large slope below the E_f along the *A*-*H* high-symmetry path in comparison with other paths in the reciprocal space. The above features are beneficial to the generation of the smaller effective electron masses. Further estimated effective electron masses corresponding to band 1 (Γ -*A*), band 2 (Γ -*A*), band 3 (*A*-*H*), and band 4 (*A*-*H*) in the selected energy range from -0.4 eV to Fermi energy are 0.999, 0.995, 0.920, and 0.830 m_0 wherein m_0 is the electron mass, respectively, indicating the relatively small electron effective mass and favoring the superconductivity of *P6/mmm* Sc₂P. Meanwhile, the clear metallicity is demonstrated, which arises from the contribution of Sc 3*d* orbital in the vicinity of the E_f [Figs. 3(a) and S8]. As illustrated in Fig. 3(b), Sc 3*d* makes a larger contribution to the metallicity of Sc₂P than Sc 4*s*, Sc 3*p*, P 3*s*, and P 3*p*, inducing the formation of van Hove singularity (vHs) slightly below the Fermi energy. Further analysis shows that there is significant overlap between Sc 3*d* and P 3*p* below the Fermi level, signifying the presence of charge transfer from Sc to P, in accordance with the computed ELF (Fig. S5) and Bader charge analysis (Table S3). Moreover, the Fermi-surface nesting along the high-symmetry *K*- Γ and Γ -*M* directions in the Brillouin zone is found via the calculated Fermi surface [Figs. 3(c) and S9] and nesting function (Fig. S10) of Sc₂P at 250 GPa. Motivated by the electronic structures features above described for the pressurized Sc₂P, we evaluate its superconducting critical temperature T_c by means of the following: the McMillan formula with the prefactor introduced by Dynes [97,98] based on BCS theory [99]:

$$T_c = \frac{\omega_{\log}}{1.2} \exp \left\{ -\frac{1.04(1 + \lambda)}{\lambda - \mu^*(1 + 0.62\lambda)} \right\}, \quad (1)$$

and the Allen-Dynes-modified McMillan equation [100] with the strong-coupling f_1 and shape f_2 correction factors is also employed:

$$T_c = f_1 f_2 \frac{\omega_{\log}}{1.2} \exp \left[-\frac{1.04(1 + \lambda)}{\lambda - \mu^*(1 + 0.62\lambda)} \right], \quad (2)$$

$$f_1 = \left[1 + \left(\frac{\lambda}{2.46(1 + 3.8\mu^*)} \right)^{3/2} \right]^{1/3}, \quad (3)$$

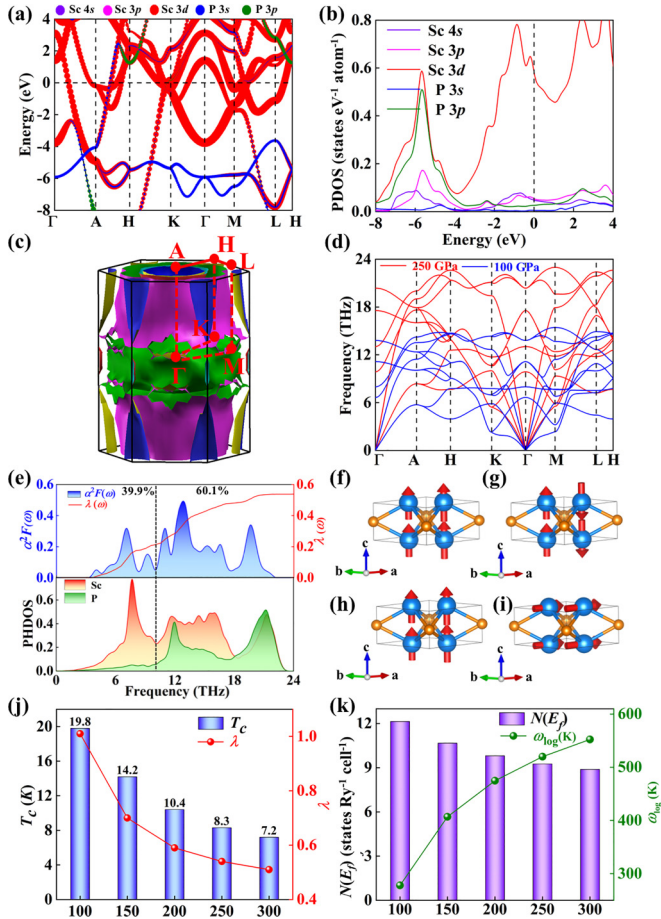


FIG. 3. Electronic and superconducting properties of $P6/mmm$ Sc_2P . (a) Orbital-resolved electronic band structure of Sc_2P at 250 GPa. Contribution of Sc and P atomic orbitals (Sc 4s, Sc 3p, Sc 3d, P 3s, and P 3p) is denoted by size of circles. Fermi energy is set to zero. (b) Projected density of states (PDOS) of Sc_2P at 250 GPa. Vertical dashed line denotes Fermi level. (c) Fermi surface of Sc_2P at 250 GPa, where red lines represent high-symmetry k -points path in Brillouin zone. (d) Phonon spectra of Sc_2P at 100 and 250 GPa. (e) Frequency-dependent Eliashberg spectra function $\alpha^2 F(\omega)$, partial electron-phonon coupling (EPC) parameter $\lambda(\omega)$, and atom decomposed phonon density of states (PHDOS) with unit of (states $\text{THz}^{-1} \text{cell}^{-1}$) of Sc_2P at 250 GPa. Vibrational modes with lowest-frequency acoustic branch at (f) H, (g) K, (h) M, and (i) L points for Sc_2P at 250 GPa are indicated by arrows. (j) Superconducting critical temperature T_c with $\mu^* = 0.10$ and integrated EPC constant λ as function of pressure. (k) Total electron density of states $N(E_f)$ at Fermi level and logarithmic average phonon frequency ω_{\log} at different pressures.

$$f_2 = 1 + \frac{(\bar{\omega}_2 - 1)\lambda^2}{\lambda^2 + [1.82(1 + 6.3\mu^*)\bar{\omega}_2/\omega_{\log}]^2}, \quad (4)$$

$$\bar{\omega}_2 = \langle \omega^2 \rangle^{1/2}. \quad (5)$$

Here, μ^* denotes the Coulomb pseudopotential with considered values of 0.10 and 0.13, ω_{\log} is the logarithmic average phonon frequency, $\bar{\omega}_2$ is mean-square frequency, and λ is the total electron-phonon coupling (EPC) constant. The partial EPC parameter $\lambda(\omega)$ as a function of frequency ω is computed

by Eliashberg spectral function $\alpha^2 F(\omega)$,

$$\lambda(\omega) = 2 \int_0^\infty \frac{\alpha^2 F(\omega')}{\omega} d\omega'. \quad (6)$$

Notably, Sc_2P is found to have a predicted T_c of 8.3 K at 250 GPa. Meanwhile, the calculated T_c value of Sc_2P at 250 GPa by solving the Eliashberg equation [101] is 9.1 K, which is slightly larger than 8.3 K estimated by the McMillan equation (Table S5). Its total EPC parameter λ is 0.54, which is comparable to 0.61 of MgB_2 [102] and is predominantly determined by the following two components. (i) The low-frequency phonon modes below 10.1 THz take on the contribution (39.9%) to the integral λ , which is mainly related to the Sc-dominated vibration. (ii) By contrast, the mixed vibrational modes of Sc and P atoms make a major contribution (60.1%) to λ in the high-frequency region above 10.1 THz, where Eliashberg spectra function $\alpha^2 F(\omega)$ shows the largest magnitude in the region of mixed Sc-P modes [Fig. 3(e)]. Based on the above, the electron-phonon interaction in $P6/mmm$ Sc_2P encompasses the whole lattice. Consequently, this superconductive mechanism of $P6/mmm$ Sc_2P is unlike those of H_3Se [103] and CaYH_{12} [104] with high-frequency modes dominated by the vibration of hydrogen atoms.

It should be noted that the robust dynamic stability and good superconductivity of some excellent superconducting materials remain kept at lower pressures [105]. For example, $Fm\bar{3}m$ LaBeH_8 is calculated to be thermodynamically stable above 98 GPa and has superconductivity of 185 K when dynamically stabilized down to 20 GPa [106]. Furthermore, it is found that the thermodynamically stable $P6/mmm$ Sc_2P phase above 212.1 GPa (Fig. S11) remains dynamically stable as pressure drops to 78 GPa due to the absence of imaginary frequency modes (Fig. S12), indicating it has metastability at lower pressure. Meanwhile, we estimated the energy barrier of Sc_2P at a selected pressure of 100 GPa using the climbing image nudged elastic band (CINEB) [107] method, where the high-pressure $P6/mmm$ and low-pressure $P6_3/m$ phases are chosen as the initial and final states for the CINEB path, respectively. The result shows that Sc_2P has an energy barrier of 151.2 meV/atom at 100 GPa (Fig. S13), implying $P6/mmm$ Sc_2P still maintains kinetic stability at relatively low pressure. Therefore, the $P6/mmm$ -structured Sc_2P synthesized at high pressure can be recovered to low pressure. With this in mind, we further investigate the pressure-dependent superconductivity of $P6/mmm$ Sc_2P . As pressure gradually decreases, T_c of Sc_2P shows remarkable enhancement (10.4 K at 200 GPa, 14.2 K at 150 GPa). Remarkably, T_c of Sc_2P can reach up to 19.8 K at 100 GPa [Fig. 3(j)], which is comparable to 22.2 K of $P6/mmm$ -structured LaP_2 at 11 GPa [35]. The resulting integrated electron-phonon coupling parameter λ also exhibits an increasing tendency (0.59 at 200 GPa, 0.70 at 150 GPa) under decompression and has a large EPC λ of 1.01 at 100 GPa [Fig. 3(j)], while the logarithmic average phonon frequency ω_{\log} is found to reduce [Fig. 3(k)]. Further superconducting mechanism analysis unveils that the contribution of the low-frequency phonon vibrations to the electron-phonon coupling strength of Sc_2P at lower pressure of 100 GPa is slightly greater than those of 250 GPa

(Fig. S14). Interestingly, the pronounced acoustic softening phonon modes of Sc_2P at 100 GPa emerge at high-symmetry H , K , M , and L points in the Brillouin zone in sharp contrast to those at 250 GPa [Fig. 3(d)], contributing to an evident increase in total EPC λ . The corresponding lowest-frequency modes related to the points of H , K , and M , and L are mainly associated with the movements of Sc atoms [Fig. 3(f)], where the Sc atoms corresponding to H , K , and M points vibrate along the c axis, whereas the modes of vibration corresponding to the L point derive from the motion of Sc atoms in the ab plane. Meanwhile, the total electron density of states of Sc_2P at the Fermi level shows an increasing tendency with decompression [Fig. 3(h)], indicating more electrons couple with the phonons and further induce the enhancement of the T_c value.

D. $I4/mmm$ Sc_3P with remarkable superconductivity

Enlightened by the record high-temperature element superconductivity recently observed in compressed elemental scandium [38,39], Sc-P phases with higher Sc concentration proposed in this work should have more outstanding superconductivity. Thereby, $I4/mmm$ -structured Sc_3P is considered for exploring the superconductive properties. Phonon calculations of $I4/mmm$ Sc_3P at 140 GPa imply that it not only maintains the dynamic stability but also possesses both marked acoustic and optical softened phonon modes in the low-frequency region along the Γ -Z direction of the Brillouin zone [Fig. 4(a)], which is in sharp contrast to that of $P6/mmm$ Sc_2P and similar to that of Al_5Si [108]. Particularly, the optical phonon softening corresponding to the Γ point at 2.2 THz is primarily ascribed to the motions of Sc1 atoms parallel to the ab plane, while the softened acoustic ones at 2.6 THz regarding the Z point also stem from the displacements of Sc1 atoms (Fig. S15). Meanwhile, the phonon branches below 14.1 THz primarily derive from the contribution of Sc1 and Sc2 atoms wherein Sc1-derived vibrations dominate, whereas the ones above 14.1 THz are mainly attributed to the vibration of P atoms, which is consistent with the analysis of the phonon density of states [Fig. 4(b)]. Furthermore, the evident flat band around the Fermi level along the A - M direction is unequivocally unveiled by the calculated electronic band structure of Sc_3P at 140 GPa, where Sc 3d undertakes the major contribution in metallicity compared to Sc 4s, Sc 3p, P 3s, and P 3p [Figs. 4(c) and S16]. Conversely, the highly dispersive bands are found in other high-symmetry directions [Fig. 4(c)]. Further decomposed PDOS analysis reveals that Sc 3d state dominates in the vicinity of the Fermi level E_f and strongly couples with P 3p within energy window from -6.0 to -4.0 eV below the E_f , supporting the strong ionic bonding between Sc and P atoms. Obviously, a vHs produced by the Sc 3d state appears at -0.6 eV below the E_f [Fig. 4(d)], which is like those of H_3S [109] and LaH_{10} [110]. The above description mentioned indicates that Sc_3P has a good potentiality in superconductivity. Remarkably, further electron-phonon coupling calculations suggest that $I4/mmm$ Sc_3P at 140 GPa is found to have a T_c value of 20.5 K, exceeding those of binary transition metal-rich phosphides [Fig. 4(h)]. Meanwhile, T_c for Sc_3P at 140 GPa is estimated to be 21 K by solving the Eliashberg equation, exhibiting slightly enhanced

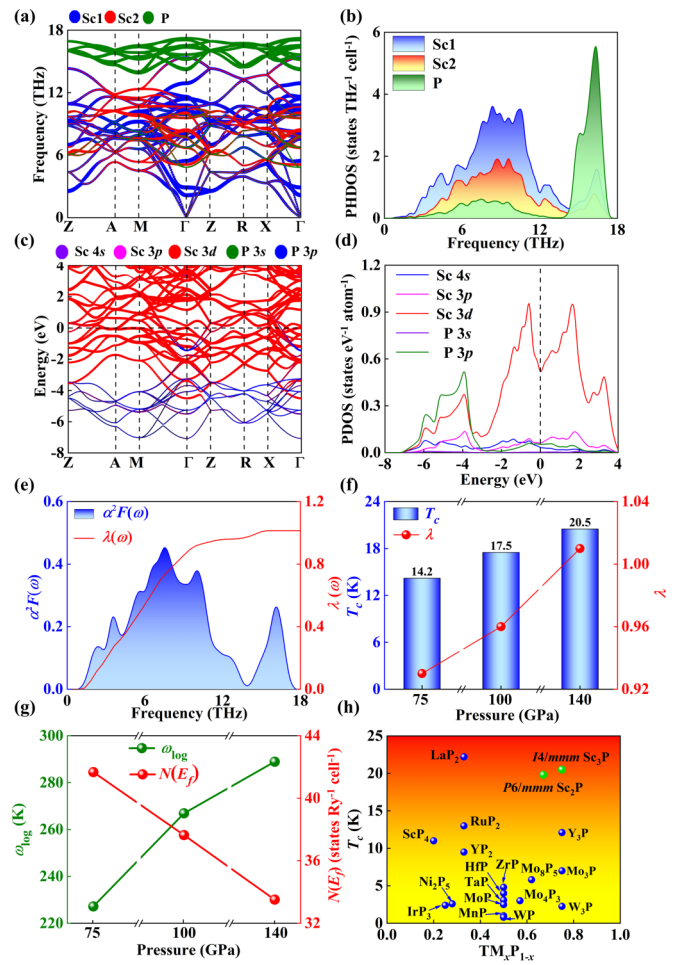


FIG. 4. Electronic structures and superconductive properties of $I4/mmm$ Sc_3P . (a) Projected phonon spectra of primitive cell of Sc_3P at 140 GPa. Size of dots in phonon dispersion curves is proportional to contribution of vibrations from Sc and P atoms (b) PHDOS of Sc_3P at 140 GPa. (c) Orbital projected band structure of primitive cell of Sc_3P at 140 GPa. Contribution of Sc and P atomic orbitals (Sc 4s, Sc 3p, Sc 3d, P 3s, and P 3p) is represented by size of circles. (d) PDOS of Sc_3P at 140 GPa. (e) Eliashberg spectra function $\alpha^2 F(\omega)$ and partial electron-phonon coupling parameter $\lambda(\omega)$ as function of frequency ω of Sc_3P at 140 GPa. (f) Pressure-dependent T_c with $\mu^* = 0.10$ and integral electron-phonon coupling constant λ . (g) Corresponding evolution of logarithmic average phonon frequency ω_{log} and total electron density of states $N(E_f)$ at Fermi energy in pressure range from 75 to 140 GPa. (h) Critical temperature T_c values of known binary superconducting transition-metal phosphides [22–24,28–35,51,112–114] as function of transition-metal concentration.

superconductivity compared to the T_c calculated by means of McMillan formula (Table S5). The corresponding electron-phonon coupling strength λ is 1.01, which is much larger than 0.61 of MgB_2 [89] at ambient pressure and elucidates that Sc_3P has sizable electron-phonon coupling interactions. Further EPC analysis suggests that the low-frequency phonon modes below 14.1 THz, chiefly related to Sc atomic vibrations, account for 94.6% of the integrated EPC parameter λ . In contrast, the P-dominated high-frequency modes above 14.1 THz make a contribution (5.4%) to λ . Thus, the strong EPC

of Sc_3P is mainly due to the coupling between Sc $3d$ electron state around E_f and Sc-derived phonons in the low-frequency region. Additionally, there are also mixed vibrational modes for Sc and P atoms in both low- and high-frequency ranges by phonon density of states (PHDOS) analysis [Fig. 4(b)], which play an important role in electron-phonon coupling, wherein the largest magnitude of Eliashberg spectra function $\alpha^2 F(\omega)$ is found to be in the region of mixed Sc-P modes [Fig. 4(e)] and further indicates the electron-phonon coupling exists in the entire frequency range.

The impact of pressure on superconductivity of $I4/mmm$ Sc_3P is further investigated. Under decompression, although the superconducting transition temperature T_c of $I4/mmm$ Sc_3P is found to suffer from suppression in comparison to that of $P6/mmm$ Sc_2P , it still keeps relatively high T_c values (17.5 K at 100 GPa, 14.2 K at 75 GPa). Correspondence to dT_c/dp slope of -0.132 K/GPa is elucidated. Further analysis indicates that the reduction of T_c values is predominantly attributed to the weakening of EPC strength λ (0.96 at 100 GPa, 0.93 at 75 GPa). Besides, the density of states at the Fermi energy $N(E_f)$ increases accompanied with decreasing pressure, indicating the noticeable enhancement of the metallicity of Sc_3P . By contrast, the logarithmic average phonon frequency ω_{\log} shows a reduced tendency. Overall, the decreasing tendency of superconductive critical temperature yielded upon releasing pressure is mainly ascribed to the synergistic effect of the EPC strength λ and ω_{\log} [Fig. 4(f)]. In addition, the study on the superconductivity of $Pbam$ ScP suggests that it has a relatively lower calculated T_c of 1.3 K at 200 GPa than those of $P6/mmm$ Sc_2P and $I4/mmm$ Sc_3P (Table S4). Moreover, the T_c values of $Pbam$ ScP, $P6/mmm$ Sc_2P , and $I4/mmm$ Sc_3P by use of the Allen-Dynes-corrected McMillan formula with the correction factors f_1 and f_2 were calculated to check their influences on the transition temperatures. The resulting T_c values of $P6/mmm$ Sc_2P and

$I4/mmm$ Sc_3P increased slightly, whereas the T_c value for $Pbam$ ScP did not change (Table S4). Meanwhile, to examine the impact of the Coulomb pseudopotential μ^* on the T_c of $Pbam$ ScP, $P6/mmm$ Sc_2P , and $I4/mmm$ Sc_3P , we calculated their T_c exploiting the McMillan equation incorporating $\mu^* = 0.13$ and found that the obtained T_c values were slightly smaller than the ones when $\mu^* = 0.10$ (Table S4). Furthermore, Debye temperatures Θ_D of $P6/mmm$ Sc_2P and $I4/mmm$ Sc_3P at different pressures were also calculated via VASPKIT [111]. The results demonstrate that Θ_D values of Sc_2P and Sc_3P show an enhanced trend induced by compression (Table S6).

IV. CONCLUSIONS

In summary, to access the promising superconductive transition-metal phosphides, we conducted a systematic exploration of scandium-rich Sc-P compounds under pressure. Three compressed phases containing ScP, Sc_2P , and Sc_3P are presented to have excellent metallicity and diverse P arrangements. Significant superconducting transition temperature is uncovered in pressurized $P6/mmm$ Sc_2P hosting the MgB_2 -type structure. Notably, Sc_3P with $I4/mmm$ symmetry is predicted to exhibit the highest superconductivity of 20.5 K among reported binary transition metal-rich phosphides so far, and further experiment is thus stimulated.

ACKNOWLEDGMENTS

The authors acknowledge the funding support from the National Natural Science Foundation of China under Grants No. 11704062 and No. 12074138, the funding from Jilin Province under Grant No. JJKH20221152KJ, the “111” Project (Grant No. B13013), and the Fundamental Research Funds for the Central Universities Grant No. 2412017QD006.

-
- [1] W. E. Pickett, Colloquium: Room temperature superconductivity: The roles of theory and materials design, *Rev. Mod. Phys.* **95**, 021001 (2023).
- [2] B. Lilia *et al.*, The 2021 room-temperature superconductivity roadmap, *J. Phys.: Condens. Matter* **34**, 183002 (2022).
- [3] J. A. Flores-Livas, L. Boeri, A. Sanna, G. Profeta, R. Arita, and M. Eremets, A perspective on conventional high-temperature superconductors at high pressure: Methods and materials, *Phys. Rep.* **856**, 1 (2020).
- [4] X. Zhou, W.-S. Lee, M. Imada, N. Trivedi, P. Phillips, H.-Y. Kee, P. Törmä, and M. Eremets, High-temperature superconductivity, *Nat. Rev. Phys.* **3**, 462 (2021).
- [5] M. Xu, Y. Li, and Y. Ma, Materials by design at high pressures, *Chem. Sci.* **13**, 329 (2022).
- [6] D. Duan, Y. Liu, Y. Ma, Z. Shao, B. Liu, and T. Cui, Structure and superconductivity of hydrides at high pressures, *Natl. Sci. Rev.* **4**, 121 (2017).
- [7] M. J. Hutcheon, A. M. Shipley, and R. J. Needs, Predicting novel superconducting hydrides using machine learning approaches, *Phys. Rev. B* **101**, 144505 (2020).
- [8] G. Gao, L. Wang, M. Li, J. Zhang, R. T. Howie, E. Gregoryanz, V. V. Struzhkin, L. Wang, and S. T. John, Superconducting binary hydrides: Theoretical predictions and experimental progresses, *Mater. Today Phys.* **21**, 100546 (2021).
- [9] C. J. Pickard, I. Errea, and M. I. Eremets, Superconducting hydrides under pressure, *Annu. Rev. Condens. Matter Phys.* **11**, 57 (2020).
- [10] X. Zhong, Y. Sun, T. Iitaka, M. Xu, H. Liu, R. J. Hemley, C. Chen, and Y. Ma, Prediction of above-room-temperature superconductivity in lanthanide/actinide extreme superhydrides, *J. Am. Chem. Soc.* **144**, 13394 (2022).
- [11] A. P. Drozdov, M. I. Eremets, I. A. Troyan, V. Ksenofontov, and S. I. Shylin, Conventional superconductivity at 203 kelvin at high pressures in the sulfur hydride system, *Nature (London)* **525**, 73 (2015).
- [12] L. Ma *et al.*, High-temperature superconducting phase in clathrate calcium hydride CaH_6 up to 215 K at a pressure of 172 GPa, *Phys. Rev. Lett.* **128**, 167001 (2022).
- [13] Z. Li *et al.*, Superconductivity above 200 K discovered in superhydrides of calcium, *Nat. Commun.* **13**, 2863 (2022).
- [14] F. Hong, L. Yang, P. Shan, P. Yang, Z. Liu, J. Sun, Y. Yin, X. Yu, J. Cheng, and Z. Zhao, Superconductivity of lanthanum superhydride investigated using the standard four-probe con-

- figuration under high pressures, *Chin. Phys. Lett.* **37**, 107401 (2020).
- [15] M. Somayazulu, M. Ahart, A. K. Mishra, Z. M. Geballe, M. Baldini, Y. Meng, V. V. Struzhkin, and R. J. Hemley, Evidence for superconductivity above 260 K in lanthanum superhydride at megabar pressures, *Phys. Rev. Lett.* **122**, 027001 (2019).
- [16] RETRACTED: N. Dasenbrock-Gammon *et al.*, Evidence of near-ambient superconductivity in a N-doped lutetium hydride, *Nature (London)* **615**, 244 (2023).
- [17] M. Sun, H. Liu, J. Qu, and J. Li, Earth-rich transition metal phosphide for energy conversion and storage, *Adv. Energy Mater.* **6**, 1600087 (2016).
- [18] Y. Shi, M. Li, Y. Yu, and B. Zhang, Recent advances in nanostructured transition metal phosphides: Synthesis and energy-related applications, *Energy Environ. Sci.* **13**, 4564 (2020).
- [19] Y. Shi and B. Zhang, Recent advances in transition metal phosphide nanomaterials: Synthesis and applications in hydrogen evolution reaction, *Chem. Soc. Rev.* **45**, 1529 (2016).
- [20] Y. Pei, Y. Cheng, J. Chen, W. Smith, P. Dong, P. M. Ajayan, M. Ye, and J. Shen, Recent developments of transition metal phosphides as catalysts in the energy conversion field, *J. Mater. Chem. A* **6**, 23220 (2018).
- [21] Y. Wang, Y. Feng, J.-G. Cheng, W. Wu, J. L. Luo, and T. F. Rosenbaum, Spiral magnetic order and pressure-induced superconductivity in transition metal compounds, *Nat. Commun.* **7**, 13037 (2016).
- [22] Z. Liu, W. Wu, Z. Zhao, H. Zhao, J. Cui, P. Shan, J. Zhang, C. Yang, P. Sun, Y. Wei *et al.*, Superconductivity in WP single crystals, *Phys. Rev. B* **99**, 184509 (2019).
- [23] Y. Li *et al.*, Concurrence of superconductivity and structure transition in weyl semimetal TaP under pressure, *npj Quantum Mater.* **2**, 66 (2017).
- [24] Z. Chi *et al.*, Pressure-Induced superconductivity in MoP, *npj Quantum Mater.* **3**, 28 (2018).
- [25] L.-M. Chen, F.-H. Wei, Y.-H. Chen, H.-Q. Liu, Y. Xu, B.-Y. Chen, C.-L. Dai, Y.-B. Zhang, and Z.-H. Yu, Superconducting and structural properties of the phosphorus-rich Nb₂P₅ superconductor under high pressure, *Tungsten* **5**, 364 (2023).
- [26] N. Gong, C. Deng, L. Wu, B. Wan, Z. Wang, Z. Li, H. Gou, and F. Gao, Structural diversity and electronic properties of 3d transition metal tetraphosphides, TMP₄ (TM = V, Cr, Mn, and Fe), *Inorg. Chem.* **57**, 9385 (2018).
- [27] K. Cao, X.-X. Qu, H. Jiang, Y.-H. Su, C. Zhang, and G. Frapper, Pressure-induced novel stable stoichiometries in molybdenum–phosphorus phase diagrams under pressure, *J. Phys. Chem. C* **123**, 30187 (2019).
- [28] X. Ma, D. Zhou, Y. Yan, J. Xu, S. Liu, Y. Wang, M. Cui, Y. Cheng, Y. Miao, and Y. Liu, Phase transition and electronic properties of skutterudite-type IrP₃ under high pressure, *Phys. Chem. Chem. Phys.* **21**, 21262 (2019).
- [29] J.-G. Cheng, K. Matsubayashi, W. Wu, J. P. Sun, F. K. Lin, J. L. Luo, and Y. Uwatoko, Pressure induced superconductivity on the border of magnetic order in MnP, *Phys. Rev. Lett.* **114**, 117001 (2015).
- [30] I. Shirovani, I. Kaneko, M. Takaya, C. Sekine, and T. Yagi, Superconductivity of molybdenum phosphides prepared at high pressure, *Phys. B: Condens. Matter* **281–282**, 1024 (2000).
- [31] T. Shang *et al.*, Nodeless superconductivity and preserved time-reversal symmetry in the noncentrosymmetric Mo₃P superconductor, *Phys. Rev. B* **99**, 184513 (2019).
- [32] W. Yang, Z. Lou, Q. Zhu, B. Chen, H. Wang, Q. Mao, J. Du, J. Yang, and M. Fang, Superconductivity in noncentrosymmetric Mo₃P single crystal, *Supercond. Sci. Technol.* **32**, 115014 (2019).
- [33] X. Liu, Z. Yu, Q. Liang, C. Zhou, H. Wang, J. Zhao, X. Wang, N. Yu, Z. Zou, and Y. Guo, High-pressure crystal growth, superconducting properties, and electronic band structure of Nb₂P₅, *Chem. Mater.* **32**, 8781 (2020).
- [34] K. Zhao, H. Yu, Q. Yang, W. Li, F. Han, H. Liu, and S. Zhang, Emerging yttrium phosphides with tetrahedron phosphorus and superconductivity under high pressures, *Chem.–Eur. J.* **27**, 17420 (2021).
- [35] X. Li, X. Zhang, Z. Yang, Y. Liu, and G. Yang, Pressure-stabilized graphene-like P layer in superconducting LaP₂, *Phys. Chem. Chem. Phys.* **24**, 6469 (2022).
- [36] J. J. Hamlin and J. S. Schilling, Pressure-induced superconductivity in Sc to 74 GPa, *Phys. Rev. B* **76**, 012505 (2007).
- [37] P. Tsuppayakorn-aek, W. Luo, W. Pongtrakoon, K. Chuenkingkeaw, T. Kaewmaraya, R. Ahuja, and T. Bovornratanaraks, The ideal commensurate value of Sc and the superconducting phase under high pressure, *J. Appl. Phys.* **124**, 225901 (2018).
- [38] J. Ying, S. Liu, Q. Lu, X. Wen, Z. Gui, Y. Zhang, X. Wang, J. Sun, and X. Chen, Record high 36 K transition temperature to the superconducting state of elemental scandium at a pressure of 260 GPa, *Phys. Rev. Lett.* **130**, 256002 (2023).
- [39] X. He *et al.*, Superconductivity above 30 K achieved in dense scandium, *Chin. Phys. Lett.* **40**, 107403 (2023).
- [40] B. Wan, Y. Lu, Z. Xiao, Y. Muraba, J. Kim, D. Huang, L. Wu, H. Gou, J. Zhang, and F. Gao, Identifying quasi-2D and 1D electrides in yttrium and scandium chlorides via geometrical identification, *npj Comput. Mater.* **4**, 77 (2018).
- [41] S. Qian, X. Sheng, X. Yan, Y. Chen, and B. Song, Theoretical study of stability and superconductivity of ScH_{*n*} (*n* = 4–8) at high pressure, *Phys. Rev. B* **96**, 094513 (2017).
- [42] L. M. McRae, R. C. Radomsky, J. T. Pawlik, D. L. Druffel, J. D. Sundberg, M. G. Lanetti, C. L. Donley, K. L. White, and S. C. Warren, Sc₂C, a 2D semiconducting electride, *J. Am. Chem. Soc.* **144**, 10862 (2022).
- [43] D. Shrivastava and S. P. Sanyal, Structural stability of scandium monochalcogenides ScS and ScSe under pressure and superconductivity: A first principles study, *Comput. Condens. Matter* **21**, e00418 (2019).
- [44] X. Ye, N. Zarifi, E. Zurek, R. Hoffmann, and N. W. Ashcroft, High hydrides of scandium under pressure: Potential superconductors, *J. Phys. Chem. C* **122**, 6298 (2018).
- [45] K. Abe, Hydrogen-rich scandium compounds at high pressures, *Phys. Rev. B* **96**, 144108 (2017).
- [46] P. Hou, F. Belli, R. Bianco, and I. Errea, Quantum anharmonic enhancement of superconductivity in P6₃/mmc Sc H₆ at high pressures: A first-principles study, *J. Appl. Phys.* **130**, 175902 (2021).
- [47] Q. Jiang, D. Duan, H. Song, Z. Zhang, Z. Huo, T. Cui, and Y. Yao, Room temperature superconductivity in Sc H₁₂ with quasi-atomic hydrogen below megabar pressure, [arXiv:2302.02621](https://arxiv.org/abs/2302.02621).

- [48] W. M. Yim, E. J. Stofko, and R. T. Smith, Vapor growth and properties of ScAs and ScP, *J. Appl. Phys.* **43**, 254 (1972).
- [49] R. Berger, Crystallographic data on new scandium arsenides and phosphides, *Acta Chem. Scand.* **34a**, 231 (1980).
- [50] R. Berger, New metal-rich phases in the scandium phosphorus system, *Acta Chem. Scand. A* **35a**, 635 (1981).
- [51] Y. Fu, F. Li, X. Zhang, S. Zhang, Y. Liu, and G. Yang, Superconducting ScP₄ with a novel phosphorus framework, *Appl. Phys. A* **128**, 318 (2022).
- [52] X. Huang *et al.*, Uncovering 0D and 1D electrides with low work function in a Sc–P system, *J. Phys. Chem. C* **126**, 20710 (2022).
- [53] L. Zhang, Y. Wang, J. Lv, and Y. Ma, Materials discovery at high pressures, *Nat. Rev. Mater.* **2**, 17005 (2017).
- [54] H.-K. Mao, X.-J. Chen, Y. Ding, B. Li, and L. Wang, Solids, liquids, and gases under high pressure, *Rev. Mod. Phys.* **90**, 015007 (2018).
- [55] A. R. Oganov, C. J. Pickard, Q. Zhu, and R. J. Needs, Structure prediction drives materials discovery, *Nat. Rev. Mater.* **4**, 331 (2019).
- [56] M. Miao, Y. Sun, E. Zurek, and H. Lin, Chemistry under high pressure, *Nat. Rev. Chem.* **4**, 508 (2020).
- [57] L. Dubrovinsky *et al.*, Materials synthesis at terapascal static pressures, *Nature (London)* **605**, 274 (2022).
- [58] Y. Wang, J. Lv, L. Zhu, and Y. Ma, Crystal structure prediction via particle-swarm optimization, *Phys. Rev. B* **82**, 094116 (2010).
- [59] Y. Wang, J. Lv, L. Zhu, and Y. Ma, CALYPSO: A method for crystal structure prediction, *Comput. Phys. Commun.* **183**, 2063 (2012).
- [60] S. Zhang, L. Zhu, H. Liu, and G. Yang, Structure and electronic properties of Fe₂SH₃ compound under high pressure, *Inorg. Chem.* **55**, 11434 (2016).
- [61] H. Zhai, R. Xu, J. Dai, X. Ma, X. Yu, Q. Li, and Y. Ma, Stabilized nitrogen framework anions in the Ga–N system, *J. Am. Chem. Soc.* **144**, 21640 (2022).
- [62] Y. Li, J. Hao, H. Liu, Y. Li, and Y. Ma, The metallization and superconductivity of dense hydrogen sulfide, *J. Chem. Phys.* **140**, 174712 (2014).
- [63] J. Lv, Y. Wang, L. Zhu, and Y. Ma, Predicted novel high-pressure phases of lithium, *Phys. Rev. Lett.* **106**, 015503 (2011).
- [64] L. Zhu, H. Wang, Y. Wang, J. Lv, Y. Ma, Q. Cui, Y. Ma, and G. Zou, Substitutional alloy of Bi and Te at high pressure, *Phys. Rev. Lett.* **106**, 145501 (2011).
- [65] H. Wang, J. S. Tse, K. Tanaka, T. Iitaka, and Y. Ma, Superconductive sodalite-like clathrate calcium hydride at high pressures, *Proc. Natl. Acad. Sci.* **109**, 6463 (2012).
- [66] Q. Yang, K. Zhao, H. Liu, and S. Zhang, Superconductive sodium carbides with pentagon carbon at high pressures, *J. Phys. Chem. Lett.* **12**, 5850 (2021).
- [67] S. Zhang, Q. Yang, X. Zhang, K. Zhao, H. Yu, L. Zhu, and H. Liu, Crystal structures and superconductivity of lithium and fluorine implanted gold hydrides under high pressures, *Phys. Chem. Chem. Phys.* **23**, 21544 (2021).
- [68] J. Zhang, H. Liu, Y. Ma, and C. Chen, Direct H–He chemical association in superionic FeO₂H₂He at deep-earth conditions, *Natl. Sci. Rev.* **9**, nwab168 (2022).
- [69] L. Liu, S. Zhang, and H. Zhang, Pressure-driven Ne-bearing polynitrides with ultrahigh energy density, *Chin. Phys. Lett.* **39**, 56102 (2022).
- [70] G. Kresse and J. Furthmüller, Efficient iterative schemes for ab initio total-energy calculations using a plane-wave basis set, *Phys. Rev. B* **54**, 11169 (1996).
- [71] P. Hohenberg and W. Kohn, Density functional theory (DFT), *Phys. Rev.* **136**, B864 (1964).
- [72] W. Kohn and L. J. Sham, Self-consistent equations including exchange and correlation effects, *Phys. Rev.* **140**, A1133 (1965).
- [73] P. E. Blöchl, Projector augmented-wave method, *Phys. Rev. B* **50**, 17953 (1994).
- [74] J. P. Perdew, K. Burke, and M. Ernzerhof, Generalized gradient approximation made simple, *Phys. Rev. Lett.* **77**, 3865 (1996).
- [75] J. P. Perdew, J. A. Chevary, S. H. Vosko, K. A. Jackson, M. R. Pederson, D. J. Singh, and C. Fiolhais, Atoms, molecules, solids, and surfaces: Applications of the generalized gradient approximation for exchange and correlation, *Phys. Rev. B* **46**, 6671 (1992).
- [76] H. J. Monkhorst and J. D. Pack, Special points for Brillouin-zone integrations, *Phys. Rev. B* **13**, 5188 (1976).
- [77] A. Togo, F. Oba, and I. Tanaka, First-principles calculations of the ferroelastic transition between rutile-type and CaCl₂-type SiO₂ at high pressures, *Phys. Rev. B* **78**, 134106 (2008).
- [78] K. Parlinski, Z. Q. Li, and Y. Kawazoe, First-principles determination of the soft mode in cubic ZrO₂, *Phys. Rev. Lett.* **78**, 4063 (1997).
- [79] P. Giannozzi, S. Baroni, N. Bonini, M. Calandra, R. Car, C. Cavazzoni, D. Ceresoli, G. L. Chiarotti, M. Cococcioni, and I. Dabo, QUANTUM ESPRESSO: A modular and open-source software project for quantum simulations of materials, *J. Phys.: Condens. Matter* **21**, 395502 (2009).
- [80] See Supplemental Material at <http://link.aps.org/supplemental/10.1103/PhysRevB.108.174513> for computational details. Phonon dispersion curves, electronic band structures, projected density of states (PDOS), electron localization function (ELF), and superconductive properties of predicted Sc-rich Sc-P phases.
- [81] J. P. Perdew, J. A. Chevary, S. H. Vosko, K. A. Jackson, M. R. Pederson, D. J. Singh, and C. Fiolhais, Erratum: Atoms, molecules, solids, and surfaces: Applications of the generalized gradient approximation for exchange and correlation, *Phys. Rev. B* **48**, 4978(E) (1993).
- [82] J. Feng, R. G. Hennig, N. W. Ashcroft, and R. Hoffmann, Emergent reduction of electronic state dimensionality in dense ordered Li–Be alloys, *Nature (London)* **451**, 445 (2008).
- [83] F. H. Spedding, J. J. Hanak, and A. H. Daane, High temperature allotropy and thermal expansion of the rare-earth metals, *J. Less Common Met.* **3**, 110 (1961).
- [84] S.-C. Zhu, X.-Z. Yan, S. Fredericks, Y.-L. Li, and Q. Zhu, First-principles investigation of Sc-III/IV under high pressure, *Phys. Rev. B* **98**, 214116 (2018).
- [85] Y. Akahama, H. Fujihisa, and H. Kawamura, New helical chain structure for scandium at 240 GPa, *Phys. Rev. Lett.* **94**, 195503 (2005).
- [86] H. Katzke and P. Tolédano, Displacive mechanisms and order-parameter symmetries for the A7-Incommensurate-Bcc

- sequences of high-pressure reconstructive phase transitions in group Va elements, *Phys. Rev. B* **77**, 024109 (2008).
- [87] A. Brown and S. Rundqvist, Refinement of the crystal structure of black phosphorus, *Acta Crystallogr.* **19**, 684 (1965).
- [88] T. Sugimoto, Y. Akahama, H. Fujihisa, Y. Ozawa, H. Fukui, N. Hirao, and Y. Ohishi, Identification of superlattice structure *cI16* in the P-VI phase of phosphorus at 340 GPa and room temperature via X-ray diffraction, *Phys. Rev. B* **86**, 024109 (2012).
- [89] J. Nagamatsu, N. Nakagawa, T. Muranaka, Y. Zenitani, and J. Akimitsu, Superconductivity at 39 K in magnesium diboride, *Nature (London)* **410**, 63 (2001).
- [90] S. Zhang, Y. Wang, G. Yang, and Y. Ma, Silicon framework-based lithium silicides at high pressures, *ACS Appl. Mater. Interfaces* **8**, 16761 (2016).
- [91] L. Zhu *et al.*, Carbon-boron clathrates as a new class of Sp^3 -bonded framework materials, *Sci. Adv.* **6**, eaay8361 (2020).
- [92] S. Zhang, X. Du, J. Lin, A. Bergara, X. Chen, X. Liu, X. Zhang, and G. Yang, Superconducting boron allotropes, *Phys. Rev. B* **101**, 174507 (2020).
- [93] A. D. Becke and K. E. Edgecombe, A simple measure of electron localization in atomic and molecular systems, *J. Chem. Phys.* **92**, 5397 (1990).
- [94] M. Rahm, R. Cammi, N. W. Ashcroft, and R. Hoffmann, Squeezing all elements in the periodic table: Electron configuration and electronegativity of the atoms under compression, *J. Am. Chem. Soc.* **141**, 10253 (2019).
- [95] C. Tantardini and A. R. Oganov, Thermochemical electronegativities of the elements, *Nat. Commun.* **12**, 2087 (2021).
- [96] R. F. W. Bader, Atoms in molecules, *Acc. Chem. Res.* **18**, 9 (1985).
- [97] W. L. McMillan, Transition temperature of strong-coupled superconductors, *Phys. Rev.* **167**, 331 (1968).
- [98] R. C. Dynes, McMillan's equation and the T_c of superconductors, *Solid State Commun.* **10**, 615 (1972).
- [99] J. Bardeen, L. N. Cooper, and J. R. Schrieffer, Theory of superconductivity, *Phys. Rev.* **108**, 1175 (1957).
- [100] P. B. Allen and R. C. Dynes, Transition temperature of strong-coupled superconductors reanalyzed, *Phys. Rev. B* **12**, 905 (1975).
- [101] G. M. Eliashberg, Interactions between electrons and lattice vibrations in a superconductor, *Sov. Phys. JETP* **11**, 696 (1960).
- [102] H. J. Choi, D. Roundy, H. Sun, M. L. Cohen, and S. G. Louie, First-principles calculation of the superconducting transition in MgB_2 within the anisotropic Eliashberg formalism, *Phys. Rev. B* **66**, 020513(R) (2002).
- [103] S. Zhang, Y. Wang, J. Zhang, H. Liu, X. Zhong, H. F. Song, G. Yang, L. Zhang, and Y. Ma, Phase diagram and high-temperature superconductivity of compressed selenium hydrides, *Sci. Rep.* **5**, 15433 (2015).
- [104] X. Liang, A. Bergara, L. Wang, B. Wen, Z. Zhao, X.-F. Zhou, J. He, G. Gao, and Y. Tian, Potential high- T_c superconductivity in $CaYH_{12}$ under pressure, *Phys. Rev. B* **99**, 100505(R) (2019).
- [105] R. Lucrezi, S. Di Cataldo, W. von der Linden, L. Boeri, and C. Heil, In-Silico synthesis of lowest-pressure high- T_c ternary superhydrides, *npj Comput. Mater.* **8**, 119 (2022).
- [106] Z. Zhang, T. Cui, M. J. Hutcheon, A. M. Shipley, H. Song, M. Du, V. Z. Kresin, D. Duan, C. J. Pickard, and Y. Yao, Design principles for high-temperature superconductors with a hydrogen-based alloy backbone at moderate pressure, *Phys. Rev. Lett.* **128**, 047001 (2022).
- [107] G. Henkelman, B. P. Uberuaga, and H. Jónsson, A climbing image nudged elastic band method for finding saddle points and minimum energy paths, *J. Chem. Phys.* **113**, 9901 (2000).
- [108] Q. Wang, K. Zhao, S. Wei, H. Liu, and S. Zhang, Crystalline aluminum silicides with electride state and superconductivity under high pressure, *Mater. Today Phys.* **28**, 100853 (2022).
- [109] W. Sano, T. Koretsune, T. Tadano, R. Akashi, and R. Arita, Effect of van Hove singularities on high- T_c superconductivity in H_3S , *Phys. Rev. B* **93**, 094525 (2016).
- [110] L. Liu, C. Wang, S. Yi, K. W. Kim, J. Kim, and J.-H. Cho, Microscopic mechanism of room-temperature superconductivity in compressed LaH_{10} , *Phys. Rev. B* **99**, 140501(R) (2019).
- [111] V. Wang, N. Xu, J.-C. Liu, G. Tang, and W.-T. Geng, VASPKIT: A user-friendly interface facilitating high-throughput computing and analysis using VASP code, *Comput. Phys. Commun.* **267**, 108033 (2021).
- [112] Q. Chen, J.-f. Wu, X.-m. Wang, C. Ding, T.-h. Huang, Q. Lu, and J. Sun, Pressure-induced superconducting and topological phase transitions in the RuX_2 ($X = P, As, Sb$) family compounds, *Prog. Phys.* **42**, 195 (2022).
- [113] A. R. Moodenbaugh, D. C. Johnston, R. Viswanathan, R. N. Shelton, L. E. DeLong, and W. A. Fertig, Superconductivity of transition metal sulfides, selenides, and phosphides with the NaCl structure, *J. Low Temp. Phys.* **33**, 175 (1978).
- [114] R. D. Blaugher, J. K. Hulm, and P. N. Yocom, Superconducting phosphides of the transition metals, *J. Phys. Chem. Solids* **26**, 2037 (1965).